CHARACTERIZATION OF THE LARGE-SCALE STRUCTURES IN AN IMPINGING ELLIPTIC JET

J. Mark Barker
Louisiana Tech University
Department of Mechanical Engineering
Ruston, Louisiana 71270, USA

James A. Liburdy
Oregon State University
Department of Mechanical Engineering
Corvallis, Oregon 97331, USA

ABSTRACT

The transport characteristics of impinging jet flows are believed to be dominated by the behaviors of the large-scale flow structures. The objective of this study is to identify and quantify the large-scale coherent structures in an impinging elliptic jet flow, based on the results of the proper orthogonal decomposition (POD) applied to instantaneous vorticity field data. A series of instantaneous velocity vector fields was determined using particle image velocimetry (PIV), and instantaneous vorticity fields were calculated. Mean and turbulent kinetic energy distributions were also determined. The flow structure characterization is primarily based on the modal energy distribution (eigenvalues) and the spatial energy distribution (eigenfunctions) results from the POD analysis. This analysis points out the differences between the flow structures in the major and minor planes of the elliptic jet, and the effects of impingement distance.

NOMENCLATURE

d	hydraulic diameter of elliptic jet orifice (m)
h	impingement distance normalized by d
r	aspect ratio of the elliptic jet orifice
tke	two-dimensional turbulent kinetic energy
u_{rms}	normalized spanwise rms velocity, major axis plane
v_{rms}	normalized spanwise rms velocity, minor axis plane
w_{rms}	normalized streamwise rms velocity
x	normalized spanwise distance, major plane
y	normalized spanwise distance, minor plane
z	normalized streamwise distance from stagnation point

INTRODUCTION

Impinging jet flows have a wide variety of applications, such as cooling or drying of materials in manufacturing processes or cooling of electronic components. The transport characteristics of impinging jet flows are believed to be strongly related to the large-scale structures present in the flow. Impinging jet flows are also found in the low-level flight envelope of V/STOL aircraft, and the strength of these large-scale structures is thought to influence the jet noise.

Elliptic jet flows form elliptic structures near the jet exit which have unique flow characteristics. As with other jet orifice shapes, the structures are convected downstream, but downstream convection for elliptic structures is non-uniform. The curvature variation of the structure results in a self-induction velocity, which contributes to the non-uniform convection of the structure. The non-uniform convection results in axes switching for the elliptic structures, where the major and minor axes of the structure reverse as it propagates downstream. For impinging elliptic jets, the extent of the downstream development of the flow structures prior to impingement and the influence on the impinging flow field is of interest. These unique flow structure behaviors have been identified by several researchers. Ho and Gutmark (1987) reported the enhanced entrainment (several times that of a circular or planar jet) of a contoured elliptic jet of aspect ratio 2. Self-induction of the elliptic structures and the associated behaviors were identified as contributing to the enhanced transport characteristics of the elliptic jet. Hussain and Husain (1989) have compared the flow structures developed for varying initial conditions for excited and unexcited elliptic jets.

Elliptic impinging jets have been shown to provide improved heat transfer at low Reynolds numbers (Owens and Liburdy, 1995), where the improved performance is thought to be related to the significantly different flow structure behaviors. Arjocu and Liburdy (1997) analyzed the complex flow behaviors in an impinging elliptic jet array, using a PIV technique to determine the velocity and vorticity distributions in the impingement region. Landreth and Adrian (1990) performed a PIV study of an impinging circular jet at low Reynolds number.

This study focuses on the identification and quantification of the flow structures in a single elliptic jet

flow field as it impinges onto a flat surface. The jet has an aspect ratio of 2 and is operated at a jet Reynolds number of 2000, with the impingement distance ranging from 2 to 6 hydraulic diameters. Instantaneous velocity vector fields were measured and instantaneous vorticity fields were calculated. The mean and fluctuating flow characteristics were determined using the time-averaged and the instantaneous velocity vector fields. Most significantly, the proper orthogonal decomposition (POD) was used to identify the modal energy distribution of the coherent flow structures in the impinging elliptic jet flow field.

EXPERIMENTAL METHODOLOGY

This experimental study was designed around the following parameters. The hydraulic diameter, d, was selected to be the characteristic length for this study. A sharp-edged elliptic orifice with a hydraulic diameter of 20 mm was used, so that there is no significant momentum thickness variation around the nozzle perimeter. The jet flow was allowed to develop naturally (without external excitation). The impingement distances, h, were selected to be 2, 4, and 6, since this range yields high heat transfer rates and the phenomenon of axis switching is expected to occur within this range. This study is a selected portion of a larger study (Barker, 1998) which included flow visualization, hot film anemometry, and particle image velocimetry (PIV).

Particle image velocimetry (PIV) was used to determine the instantaneous velocity vector fields in the major and minor axis planes of the impinging elliptic jet flow field. A frequency-doubled, pulsed Nd:YAG dual laser with a pulse duration of approximately 6 ns was used to illuminate the flow field. The time delay between the pulses from each of the dual lasers was variable from 100 ms to 100 ns. A high-speed digital camera and a commercially available software package were used to determine the instantaneous velocity vector fields using a cross-correlation technique. The flow was seeded with 32 μm diameter hollow polystyrene spheres containing a fluorescent dye tuned to the frequency of the illuminating laser. The field of view for the PIV was approximately 3d by 3d, extending from the stagnation point, including one half of the impingement region, with the bottom of the field of view being coincident with the impingement surface.

For each set of experimental conditions (Re, r, h, and axis plane), the data were captured in time sequences of 7 instantaneous velocity vector fields per sequence, with the time separation between fields determined by the laser repetition rate of 10 Hz. The number of fields was limited by the amount of RAM available in the host computer. Forty-nine instantaneous velocity vector fields, or 7 different time sequences, were captured for each experimental condition. The instantaneous vorticity fields and the mean velocity fields were calculated from each of the 49 instantaneous velocity fields. The mean kinetic energy was determined from the mean velocity fields, while the fluctuating field information, such as rms velocity components, was determined from the mean and instantaneous velocity fields. The results of the proper orthogonal decomposition (POD) analysis of the instantaneous vorticity squared fields are used to determine characteristics of the large-scale structures.

Proper Orthogonal Decomposition

The primary goal of this study is to identify and quantify the large-scale structures in the impinging elliptic jet flow field. Turbulent structures and their coherent nature in several different types of flows have been represented by concentration of vorticity (Hussain, 1986). Qualitative identification of large-scale structures is often based on regions of circulating or swirling flow as shown by flow visualization. Quantitative data can be obtained from PIV results, but with these data, an objective technique for identifying and quantifying flow structures is necessary. Other studies have used conditional sampling to identify the structures, but this technique requires some assumptions about the flow structures to be identified in order to determine the selection criteria.

The proper orthogonal decomposition (POD) is a mathematical tool for obtaining low-dimensional models from complex systems. The POD decomposes an ensemble of instantaneous flow fields into an orthogonal set of deterministic functions or modes. These modes have a maximum energy content, which ensures that a minimum number of modes are required to represent the flow characteristics.

The POD was introduced in the study of turbulence by Lumley (1967). Other researchers have followed, applying the POD to such flows as boundary layer, channel, and to PIV data from a Blasius flow (Wiegel, 1995). As applied to fluid mechanics, the procedure is designed to determine coherent structures by decomposing (or expanding) the flow field variable into a set of Karhunen-Loève eigenfunctions. These functions require no prior specification, and the result of the process represents the energy of the signal in the fewest number of modes. This method is completely objective and optimally efficient.

The proper orthogonal decomposition (POD) is used in this study to objectively identify and quantify large-scale structures in the impinging elliptic jet flow field. The data selected for this POD analysis is the ensemble of the instantaneous vorticity squared fields. The vorticity squared (ω^2) was selected in order to represent the vortical structures in the flow field. The results of the POD analysis of ω^2 represent the concentrations of energy in ω^2. The selection of ω^2 provides a means of identifying coherent structures corresponding to spatial concentrations of ω^2. The instantaneous velocity fields generated by the PIV method provide this unique capability to determine the instantaneous vorticity field, and to identify the coherent structures from the POD analysis.

The ensemble of the instantaneous vorticity fields, ω^2, is decomposed into an orthogonal set of deterministic functions, σ, also referred to as modes or eigenfunctions, which represent the flow structures. The uniqueness of this set of functions is that the resulting modes have maximum energy content of ω^2, and the efficiency of the method is that the energy of the ω^2 is stored in a minimum number of modes. Further details of this particular application of the POD to the identification of large-scale structures can be found in (Barker, 1998).

The solution of the eigenvalue problem associated with the large-scale structure identification using the POD

analysis results in a set of eigenvalues (λ) and eigenfunctions (σ). The individual eigenvalues λ_i are ordered by decreasing magnitude, and are ensured to be positive by the form of the kernel. The eigenvalues represent the modal energy distribution of the ω^2 energy. The individual eigenfunctions σ_i are associated with the corresponding eigenvalue λ_i and represent the spatial distribution of the energy contained in any mode i.

Two regions of the flow field were selected for the POD analysis. Region one includes the development of the jet flow into the impingement region (impinging jet region) and region two includes the flow development along the impingement surface (wall jet region). Region one contains the shear layer of the impinging jet and extends from the stagnation point approximately 2 d towards the jet exit plane (in the z direction) and approximately 1.25 d in the spanwise (x or y) direction. Region two contains the developing wall jet flow and extends from the stagnation point 1.25 d in the z direction and 2.5 d in the spanwise (x or y) direction. Both of these regions include the impingement region.

The validity of the POD computational process was established by reconstructing several instantaneous vorticity squared fields using the POD results. The criteria used was that the number of modes (typically about 50) used in the reconstruction contain 99% of the total energy in the vorticity squared signal.

As has been shown in the literature, the first mode of the POD results corresponds to the mean behavior of the flow. Figure 1 compares the spatial distribution of the first mode eigenfunction with the measured mean vorticity squared in region one for an impingement distance of h=2. (The stagnation point is located at coordinates (0,0).) The agreement between the eigenfunction and the mean vorticity squared in this region is excellent, with the spatial distributions being the same except near the spanwise edge of the region. The magnitudes cannot be compared directly, as the eigenfunction has been normalized. Similar results were evident in region two, as well as for the impingement distances of h=4 and 6.

RESULTS AND DISCUSSION

The results of this experimental study provide a unique data set for the study of an impinging elliptic jet flow field. The data analysis is based on the results of PIV full field data which is used to analyze both mean and fluctuating components of the flow. Also presented are the results from the proper orthogonal decomposition (POD), indicating the modal and spatial energy distribution of the vorticity squared. These data are used to study the dynamic structures in the impinging elliptic jet flow field.

In the normalized mean velocity fields for the major and minor axis, for the impingement distance of h=2, the deceleration of the jet in the axial, or z, direction is clearly evident in the impingement region. Also evident is the acceleration of the fluid in the jet shear layer through the impingement region, and the growth of the developing wall jet along the impingement surface. These results demonstrate the converging of the velocity vectors toward the jet axis in the major axis plane and the spreading of the velocity vectors away from the axis in the minor plane. This flow pattern is consistent with the expected axis switching for an elliptic jet. The decay of the potential core and the growth of the shear layer are evident in the mean velocity fields for h=4 and 6. These data also indicate continued spreading and converging in the minor and major planes, respectively. The mean flow field was further studied using flow visualization (Barker, 1998), which confirms the interpretation of these PIV results.

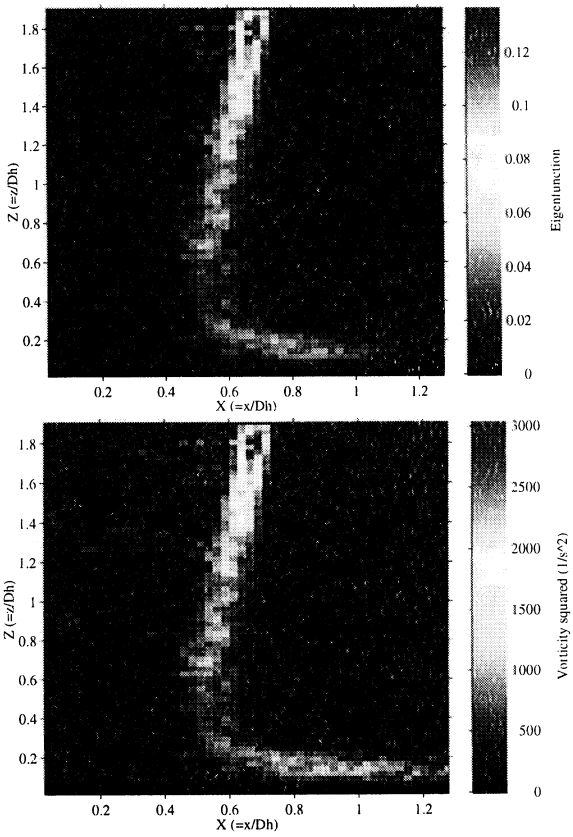

Figure 1. Comparison of mode one and mean ω^2.

The asymmetric behavior of the impinging elliptic jet is further demonstrated by the variation in the growth of the shear layer in the major and minor planes. The thickness of the shear layer was determined using the locations where the streamwise velocity component was 95% and 25% of the local centerline velocity. The growth of the shear layer was measured based on the slope of the shear layer thickness versus the downstream distance from the jet exit plane. These data are presented in Fig. 2 for the major and minor axis planes. It can be seen that the growth rate of the shear layer in the minor plane is greater than in the major plane. Also, the shear layer growth rate declines with increasing h in the minor plane, while it increases with increasing h in the major plane. The minor plane shear layer growth rate is about 3 times the major plane for h=2, and about 1.5 times for h=6. Consequently, it is seen that the converging flow in the major axis plane results in a thickening of the shear layer, with the opposite effect in the minor axis plane. As

the impingement distance increases, the rate of change increases.

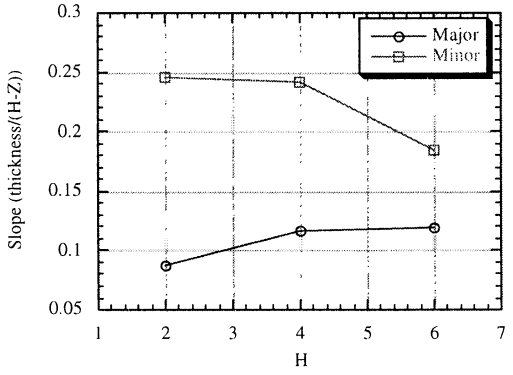

Figure 2. Shear layer growth rate.

The mean kinetic energy (mke) was calculated from the mean streamwise and spanwise velocity components, and the spatial distribution of the mean kinetic energy is shown for the major and minor axis planes at h=2 in Fig. 3. The shear layer can be clearly seen as the interface between the potential core of the jet and the surrounding quiescent fluid. The increase in mean kinetic energy associated with the acceleration of the jet flow into the developing wall jet region is evident, and appears to be greater in the minor plane than in the major plane.

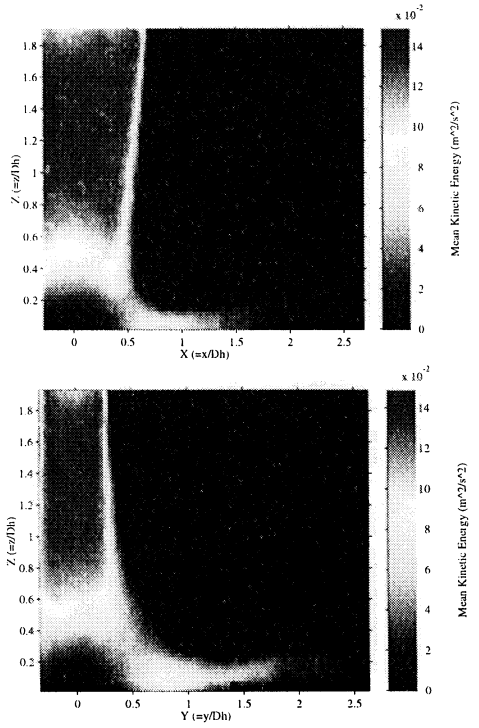

Figure 3. Major and minor plane mke distribution (h=2).

The velocity field data was used to calculate statistical flow quantities, such as rms velocity and two-dimensional turbulent kinetic energy, at each data location within the velocity field. The spatial distribution of the rms velocity for the streamwise (w_{rms}) and spanwise (u_{rms} or v_{rms}) velocity components was determined from the velocity field data. The rms velocity fields are viewed as a measure of the spatial concentrations of turbulent flow. The two-dimensional turbulent kinetic energy (tke) was calculated from the streamwise and spanwise rms velocities. The spatial distribution of the tke for the major and minor axis planes at h=2 is shown in Fig 4.

There is a spatial concentration of tke in the region where the shear layer of the free jet is located. The magnitude of the streamwise rms velocity in this region is greatest near the jet exit, and decays beyond about 0.5 diameters downstream. In contrast, the magnitude of the spanwise rms velocity increases in the region of the shear layer beyond about 0.5 diameters downstream of the jet exit. Similar behavior is seen in the streamwise and spanwise rms velocity distributions for the minor plane at h=2. These results indicate that turbulence is being transmitted from the streamwise to the spanwise velocity component in both the major and minor planes.

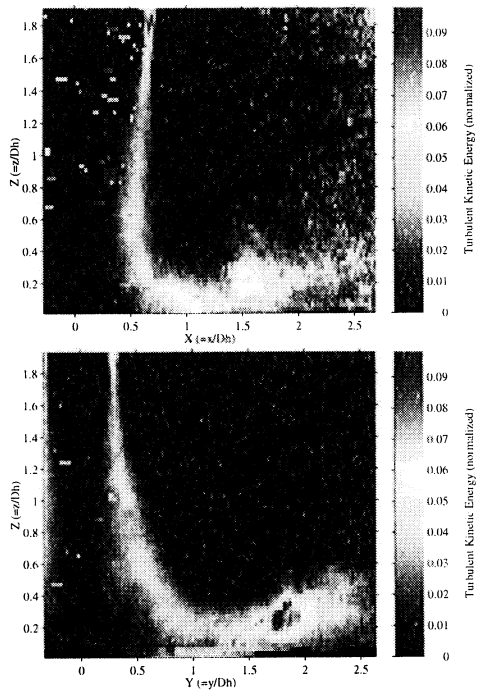

Figure 4. Major and minor plane tke distribution (h=2).

The tke in the developing wall jet region for both the major and minor planes at h=2 has a significant spatial concentration between 1.5 and 2 diameters in the spanwise direction from the stagnation point. This is taken to be indicative of a vortical structure in this location (shown later). In fact, the process of axis switching (coupled with impingement region effects) can be detected here, as the structure location in the minor plane is already (at h=2)

farther from the stagnation point in the spanwise direction, consistent with axis switching of the elliptic vortical structure. The spanwise rms velocity distribution indicates an overall increase in this component of the turbulence in the developing wall jet region.

The results of the POD include the eigenvalues (λ_i), which represent the modal distribution of the total energy in ω^2 in mode i, and the eigenfunctions (σ_i), which represent the spatial distribution of the ω^2 energy in mode i. The first mode represents the energy distribution of the mean value of ω^2, as was seen in Fig. 1. The second and higher modes are interpreted as flow structures, which may be consistent with the idea of a distribution of coherent structures. The second mode corresponds to the largest, or most energetic, structures, while the higher order modes represent successively less energetic structures. The spatial distribution of the energy in a particular mode provides further indication of the organized structures, where spatial concentrations of the ω^2 energy distributions correspond to organized flow structures.

The modal energy distributions of ω^2 in regions one and two for h=2 in the major and minor planes are compared in Fig. 5, where the energy content is related to mode number. The symbol "h2" corresponds to impingement distances of h = 2; "j" and "n" refer to the major and minor axis planes, respectively; and "r1" and "r2" refer to POD regions one and two, respectively. The first mode energy content in region one (impinging jet region) in the major axis plane is significantly higher than in the minor plane. This indicates a higher level of mean vorticity concentration in the major plane of the impinging jet region. This increased vorticity in the major plane is also evident in the higher order modes. The differences between the magnitudes of the first mode and the magnitudes of the second and higher order modes indicates the level of turbulence associated with the vorticity in the flow regions. For the wall jet region (region two), the energy level in the first and higher order modes is higher in the minor plane than in the major plane. Based on this, there is significantly greater concentration of vorticity in the minor plane of the wall jet region at h=2.

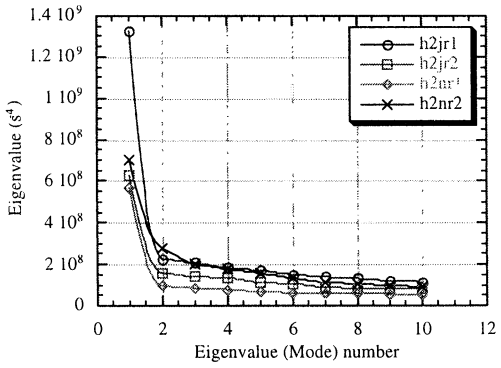

Figure 5. Modal energy distribution, h=2.

The modal energy distributions for h=4 in the impinging jet region show that the energy content of the first mode is essentially identical for both the major and minor planes, indicating an equalization of the mean vorticity distribution between these two planes. For the higher order modes, the energy level in the minor axis plane is higher than for the same mode in the major plane, which is a reversal of the results for h=2. Consequently, as axis switching is beginning to occur, there is an increased vorticity concentration in the minor plane. In the wall jet region, the first mode has more energy in the minor axis plane, while the higher order modes have approximately the same energy level in the major and minor planes. The modal energy distributions for h=6 also show behaviors consistent with axis switching. The first mode in the impinging jet region of the minor axis plane has a larger energy content of ω^2 than in the major plane, so the dominant energy is found in the minor plane for h=6, but in the major plane for h=2. In the wall jet region at h=6, the energy content of the ω^2 is larger in the major plane, which again differs from the results for h=2 and 4 in the same region.

Spatial concentrations of the eigenfunctions (σ_i) in the higher order (i>1) modes indicate concentrations of the energy of ω^2. Each eigenfunction has been self-normalized, so direct comparisons of the magnitudes of the modal energy content of ω^2 cannot be made. However, the overall energy content decreases with increasing mode number, as measured by λ_i. The spatial distributions of modes 2 and 4 in the wall jet region (region 2) of the major axis plane are shown in Fig. 6 for h=2. Spatial concentrations of ω^2 are evident in the region where the impinging jet shear layer accelerates through the stagnation region. In this region, it was also observed during the flow visualization studies that large-scale flow structures periodically emerged and decayed (Barker, 1998). The spatial concentration in mode 2 also corresponds to the location of the vortical structure identified in the tke for the major plane at h=2. Note that the spatial concentration in mode 4 is confined to a smaller region than that in mode 2, which suggests that the structure is smaller as well as less energetic. In general, the size of the structures can be estimated from the spatial concentration of the ω^2 energy distribution. The structures indicated in mode 4 are estimated to be about 0.23 d in diameter, or approximately 5 mm. This structure size agrees very closely with rough size estimates (about 6 mm) determined from the flow visualization data for intermittent structures found in this region of the flow.

These data also suggest that there are structures of different size and energy in approximately the same spatial location. This illustrates the possible spatially local cascade of energy through turbulent scales. This process appears to occur relatively rapidly, as strong convection downstream is not evident. That is to say that the local time scale of energy cascade is small compared to the mean convective time scale.

Spatial distributions of ω^2 for higher order modes were also determined for regions one and two in the minor axis plane for h=2, and in both planes for h=4 and 6. In general, the spatially intermittent coherent structures are found in the region of the shear layer of the flow field. As the impingement distance increases, the locations of these structures are more widely distributed in the flow,

corresponding to the similar spreading associated with the behavior of the shear layer. It appears for higher mode numbers, the structures in the flow are spatially more intermittent. In the wall jet region, the magnitude of the spatially concentrated ω^2 decreases with increasing h, indicating a significant decay of energy.

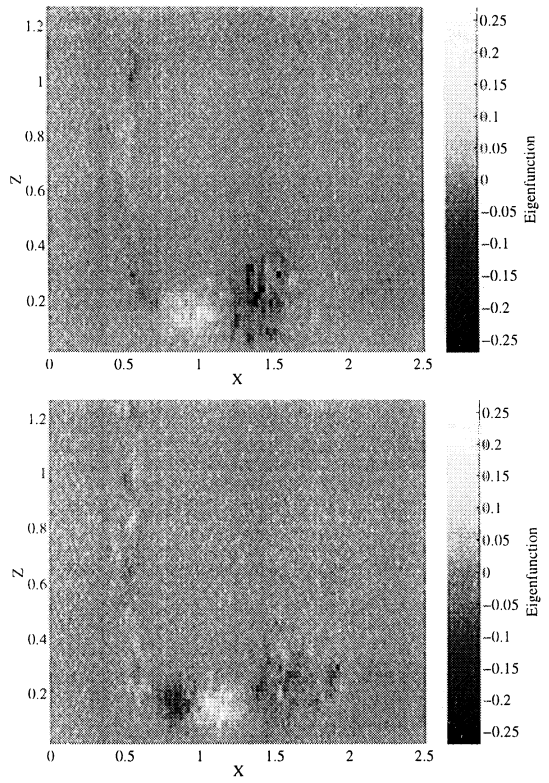

Figure 6. Higher order modes (2, 4), h=2, major axis, region two.

The mean flow data has demonstrated the spreading and converging of the elliptic jet flow in the minor and major axis planes. The location and mean behavior of the shear layer is easily noticed. The tke distribution has proved useful in identifying the location of large-scale structures in the developing wall jet region of the flow, which correspond to structures also identified using flow visualization. The location of these structures indicate that they are associated with the axis switching process The results of the proper orthogonal decomposition (POD) have demonstrated the ability to objectively identify coherent vortical structures of varying energy content in the flow based on the spatial distribution of the ω^2 energy.

CONCLUSIONS

The mean and fluctuating characteristics of an impinging elliptic jet flow field have been determined using the PIV measurement technique. These characteristics, for example the spreading and converging of the jet in the minor and major planes, have been found to agree with the known behaviors and previous measurements of the free elliptic jet. The resulting full field PIV data provides additional detailed information as compared to traditional point measurement techniques. The full field fluctuating data show that the vortical structures are represented by the spatial distribution of the turbulence. The vorticity fields were analyzed using POD to objectively determine information about the vortical structures through the spatial distribution of the vorticity squared. The results of the POD were found to support the axis switching behavior reported in other studies, demonstrated here by the variation in the strength of the first mode. The existence of coherent structures of different energy levels was indicated by the spatial concentrations of the eigenfunctions and the modal energy distribution obtained from the POD. These coherent structures were identified from the spatial concentrations of the ω^2 energy in the higher order modes. These structures are distributed throughout the higher order modes, indicating the cascade of energy through turbulent structures. Generally, the magnitude of the coherent structures in the wall developing region is greater than in the impingement region. The axis switching process indicates a clear redistribution of the energy concentration in the fluctuating vorticity in the major and minor planes.

REFERENCES

Arjocu, S. C., and Liburdy, J. A., "Analysis of Flow Structures Occurring in Impingement of Elliptic Jet Arrays," in *28th AIAA Fluid Dynamics Conference*, Snowmass Village, CO, AIAA Paper No. 97-1993.

Barker, J. M., 1998, "Flow Structure Dynamics of an Impinging Elliptic Jet," Ph. D. Dissertation, Clemson University, Clemson, SC.

Ho, C. M., and Gutmark, E., 1987, "Vortex induction and mass entrainment in a small-aspect-ratio elliptic jet," *Journal of Fluid Mechanics*, Vol. 179, pp. 383-405.

Hussain, A. K. M. F., 1986, "Coherent Structures and Turbulence," *Journal of Fluid Mechanics*, Vol. 173, pp. 303-356.

Hussain, F., and Husain, H. S., 1989, "Elliptic jets. Part 1. Characteristics of unexcited and excited jets," *Journal of Fluid Mechanics*, Vol. 208, pp. 257-320.

Landreth, C. C., and Adrian, R. J., 1990, "Impingement of a Low Reynolds Number Turbulent Circular Jet onto a Flat Plate at Normal Incidence," *Experiments in Fluids*, Vol. 9, pp. 74-84.

Lumley, J. L., 1967, "The structure of inhomogeneous turbulent flows," *Atmospheric Turbulence and Radio Wave Propagation*, pp. 166-178.

Owens, R. D., and Liburdy, J. A., 1995, "Effect of Nozzle Geometry on Impingement Heat Transfer Distribution from Jet Arrays," ASME *National Heat Transfer Conference Proceedings*.

Wiegel, M., and Fischer, M., 1995, "Proper orthogonal decomposition applied to PIV data for the oblique transition in a Blasius boundary layer," *Optical Techniques in Fluid, Thermal, and Combustion Flow*, SPIE, San Diego, CA.